ACS APPLIED ELECTRONIC MATERIALS

pubs.acs.org/acsaelm

Spotlight on Applications

# Gadolinium Halide Monolayers: A Fertile Family of Two-Dimensional 4f Magnets

Haipeng You, Ning Ding, Jun Chen, Xiaoyan Yao,* and Shuai Dong*

Cite This: *ACS Appl. Electron. Mater.* 2022, 4, 3168−3176

Read Online

ACCESS | Metrics & More | Article Recommendations

**ABSTRACT:** Two-dimensional (2D) magnets have great potentials for applications in next-generation information devices. Since the recent experimental discovery of intrinsic 2D magnetism in monolayer $CrI_3$ and few-layer $Cr_2Ge_2Te_6$, intense studies have been stimulated in pursuing more 2D magnets and revealing their intriguing physical properties. In comparison to the magnetism based on 3d electrons, 4f electrons can provide larger magnetic moments and stronger spin−orbit coupling but have been much less studied in the 2D forms. Only in very recent years have some exciting results been obtained in this area. In this mini-review, we will introduce some recent progress in 2D Gd halides from a theoretical aspect. It is noteworthy that 4f and 5d orbitals of Gd both play key roles in these materials. For $GdX_2$ (X = I, Br, Cl, F) monolayers and related Janus monolayers, robust ferromagnetism with large exchanges comes from the $4f^7 + 5d^1$ hybridization of $Gd^{2+}$. The spatially expanded 5d electrons act as a bridge to couple localized 4f spins. For $GdX_3$ monolayers, the intercalation of metal atoms can dope electrons into Gd's 5d orbitals, which leads to numerous intriguing physical properties, such as ferroelasticity, ferromagnetism, and anisotropic conductance. In brief, Gd halides establish an effective strategy to take advantage of f-electron magnetism in 2D materials.

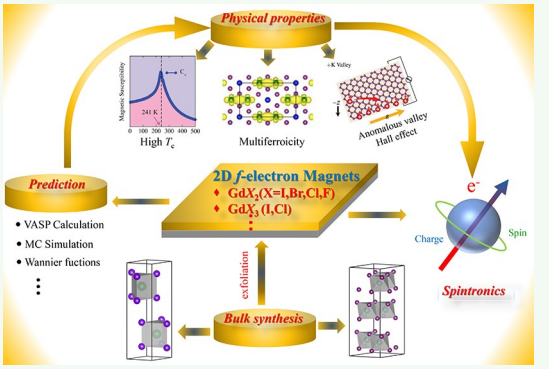


**KEYWORDS:** *4f-magnet, Gd halide, two-dimensional magnet, Janus monolayer, anisotropic conductance, structural reconstruction, double exchange*



## 1. INTRODUCTION

In 2004, as a true two-dimensional (2D) material, single-layer graphene was successfully isolated from graphite,[1] thus opening a new door to pursue high-performance 2D materials for diversified device applications.[2−13] During the past decade, the scope of 2D materials has been expanded rapidly, covering numerous famous materials including black phosphorus,[14,15] hexagonal boron nitride (*h*-BN),[16] metal oxides,[17] transition-metal dichalcogenides (TMDs),[18−27] and so on. Their excellent physical properties bring more possibilities of further miniaturization and high integratablility for nanoelectronic devices.

In the field of 2D materials, research on magnetism is always a highlighted topic due to its potential application to spintronics and electronics.[28−35] In 2017, a breakthrough was achieved: that is, intrinsic ferromagnetism was experimentally discovered in monolayer $CrI_3$ and few-layer $Cr_2Ge_2Te_6$.[36,37] Both of them are ferromagnetic (FM) insulators with a low Curie temperature ($T_C$): namely, $T_C$ = 45 K for the $CrI_3$ monolayer and $T_C$ = 28 K for the $Cr_2Ge_2Te_6$ bilayer. Soon afterward, a $Fe_3GeTe_2$ monolayer was reported to be a conductor with intrinsic ferromagnetism, whose $T_C$ value could be modulated by ionic gating.[38] Subsequently, a large number of various 2D magnets, including FM semiconductors (e.g., $MnSe_2$,[27] $VSe_2$[39]), antiferromagnetic (AFM) semiconductors (e.g., $MnPS_3$,[40] $FePS_3$[25]), and FM metals (e.g., CrB,[41] MnX (X = P, As)[42]), have been synthesized by using mechanical cleavage, molecular beam epitaxy, or chemical vapor deposition.

In terms of the theoretical design of 2D magnets, there are generally two classes of approaches. One approach is to search for 2D intrinsic magnetic materials with magnetic ions, especially van der Waals (vdW) layered magnets.[28,29,43] Then monolayer and few-layer 2D magnets can be obtained by mechanical exfoliation. The other approach is to pursue improper 2D magnetic systems, that is, to introduce spin polarization into nonmagnetic materials. It can obtained via many methods, such as doping with few magnetic atoms, creation of some edge/defects with unpaired electrons, strain engineering, heterojunction construction, and so on.[44,45]

**Special Issue:** 2D Magnetism - Materials, Devices, and Applications

**Received:** March 25, 2022
**Accepted:** April 28, 2022
**Published:** May 17, 2022

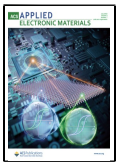




https://doi.org/10.1021/acsaelm.2c00384
*ACS Appl. Electron. Mater.* 2022, 4, 3168−3176

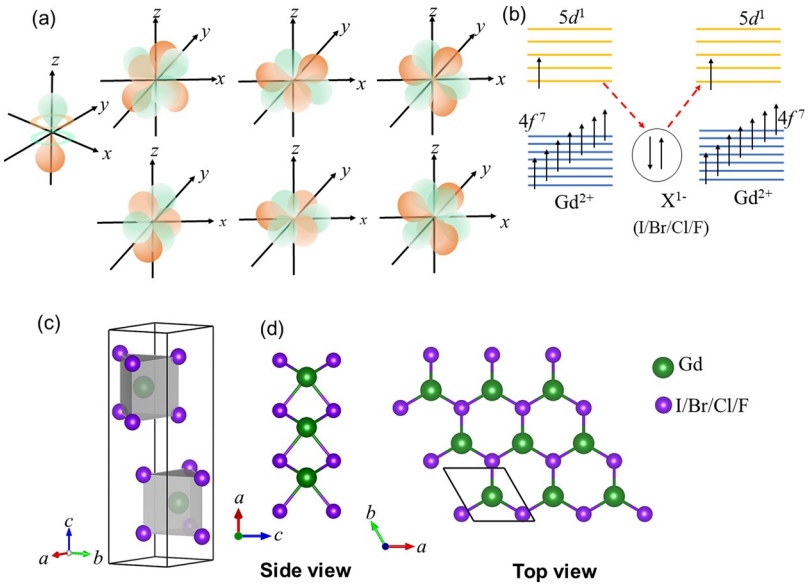


**Figure 1.** (a) Graphic of 4f orbitals. (b) Schematic diagram of a double-exchange-like mechanism for $GdX_2$ (X = I, Br, Cl, F) monolayers. (c) Crystal structure of vdW layered bulk $GdI_2$ with the $P6_3/mmc$ phase. (d) Side and top views of monolayer $GdX_2$.

The aforementioned 2D magnets, no matter whether they have been experimentally verified or theoretically predicted, are mostly based on spin moments of 3d electrons. Alternatively, here we will provide an overview of recent theoretical progress on another branch, i.e. the 2D Gd halides, and focus on their unique 4f-electron magnetism and related fascinating physical properties, such as ferrovalley and ferroelasticity. In the following, this review is divided into three parts. The first part will describe the studies on 2D FM $GdX_2$ (X = I, Br, Cl, F).[46−50] The second part will recall Gd dihalide based Janus monolayers, including GdClF, GdBrCl, GdICl, and GdIBr.[51,52] The third part will introduce 2D $GdI_3$ and $GdCl_3$ monolayers, as well as their variants with metal atom intercalation.[53,54] It is noteworthy that the 4f and 5d orbitals of Gd both play crucial roles in these materials. For $GdX_2$ and related Janus monolayers, the spatially expanded 5d electrons act as a bridge to couple localized 4f spins, and their $4f^7 + 5d^1$ hybridization of $Gd^{2+}$ leads to large exchange interactions, as illustrated in Figures 1a,b. For $GdI_3$ and $GdCl_3$ monolayers, the intercalation of Li or Mg atoms can dope electrons into Gd's 5d orbitals, which induces a Peierls transition and prominent ferroelasticity, or significant structural reconstruction with ferromagnetism and anisotropic electrical transport.

In comparison with the extensively studied 2D magnets with 3d electrons, the 4f electrons in 2D materials may provide much stronger spin−orbit coupling (SOC) and much larger local magnetic moment but have been much less studied to date. Therefore, studies on 2D 4f-electron magnets are just in the very early stage, with limited literature. Generally speaking, 4f orbitals are always too localized spatially, and thus the exchanges between neighboring 4f spins are typically weak. It is interesting and important to learn how to use the advantages of 4f electrons and circumvent their weaknesses. In particular, the Gd-based halide monolayers may be the most studied series, with corresponding vdW bulks being given in experiments and theoretical reports. In comparison with other 4f magnets, some Gd-based magnets can show much higher magnetic ordering temperatures, thanks to the help of its 5d orbitals. Furthermore, many other rare-earth elements, with non-half-filled 4f orbitals, are hard to treat in first-principles calculations. For these reasons, our current mini-review will focus mainly on Gd-based halides, which is a starting point for the studies of 2D 4f magnets. Our mini-review can shed light on the manipulation of the 4f-electron magnetism in 2D systems and its related applications.

## 2. GADOLINIUM DIHALIDE: $GdX_2$ (X = I, Br, Cl, F) MONOLAYER

Bulk $GdI_2$ with a vdW layered structure was first synthesized by Mee and Corbett et al. in 1965,[55] and it possesses a FM order with $T_C$ values up to room temperature (300−340 K).[56−58] As shown in Figure 1c, the $GdI_2$ bulk consists of I−Gd−I sandwich layers with the 2H-$MoS_2$-type structure, and these layers stack along the *c* axis in an AB sequence. Each Gd ion is caged within a triangular prism formed by six I ions, and in each layer Gd ions constitute a triangular lattice (Figure 1d). Except for $GdI_2$, no experiment has been reported so far regarding other $GdX_2$ species (X = Br, Cl, F).

In 2020, 2D monolayer $GdI_2$ was predicted to be a FM semiconductor with a $T_C$ value close to ambient temperature.[46] Following this pioneering work, other $GdX_2$ (X = Br, Cl, F) monolayers with the identical in-plane structure (Figure 1d) were explored by theoretical calculations.[47−49] Their stabilities were confirmed by elastic property calculations and *ab initio* molecular dynamics (AIMD) simulations. The estimated cleavage energy for $GdI_2$ is 0.26 J/m$^2$, which is less than that of graphite, indicating the experimental feasibility of exfoliating a $GdI_2$ monolayer from its layered bulk.[46] The cohesive energies 5.52, 4.42, and 4.01 eV per atom for $GdF_2$, $GdCl_2$, and $GdBr_2$, respectively, are smaller than that of graphene but larger than that of $Cu_2Ge$, implying the great possibility for them to be captured experimentally.[48]

According to the theoretical calculations,[46−50] all $GdX_2$ monolayers are FM semiconductors with a large magnetic moment 8 $\mu_B$/fu (fu = formula unit), and they all display a typical bipolar magnetic feature. With the $GdI_2$ monolayer as an example, as plotted in Figure 2a, the top valence band and the bottom conduction band possess an inverse spin-polarization orientation, enabling the feasibility to gain half-metallicity and


https://doi.org/10.1021/acsaelm.2c00384
ACS Appl. Electron. Mater. 2022, 4, 3168−3176

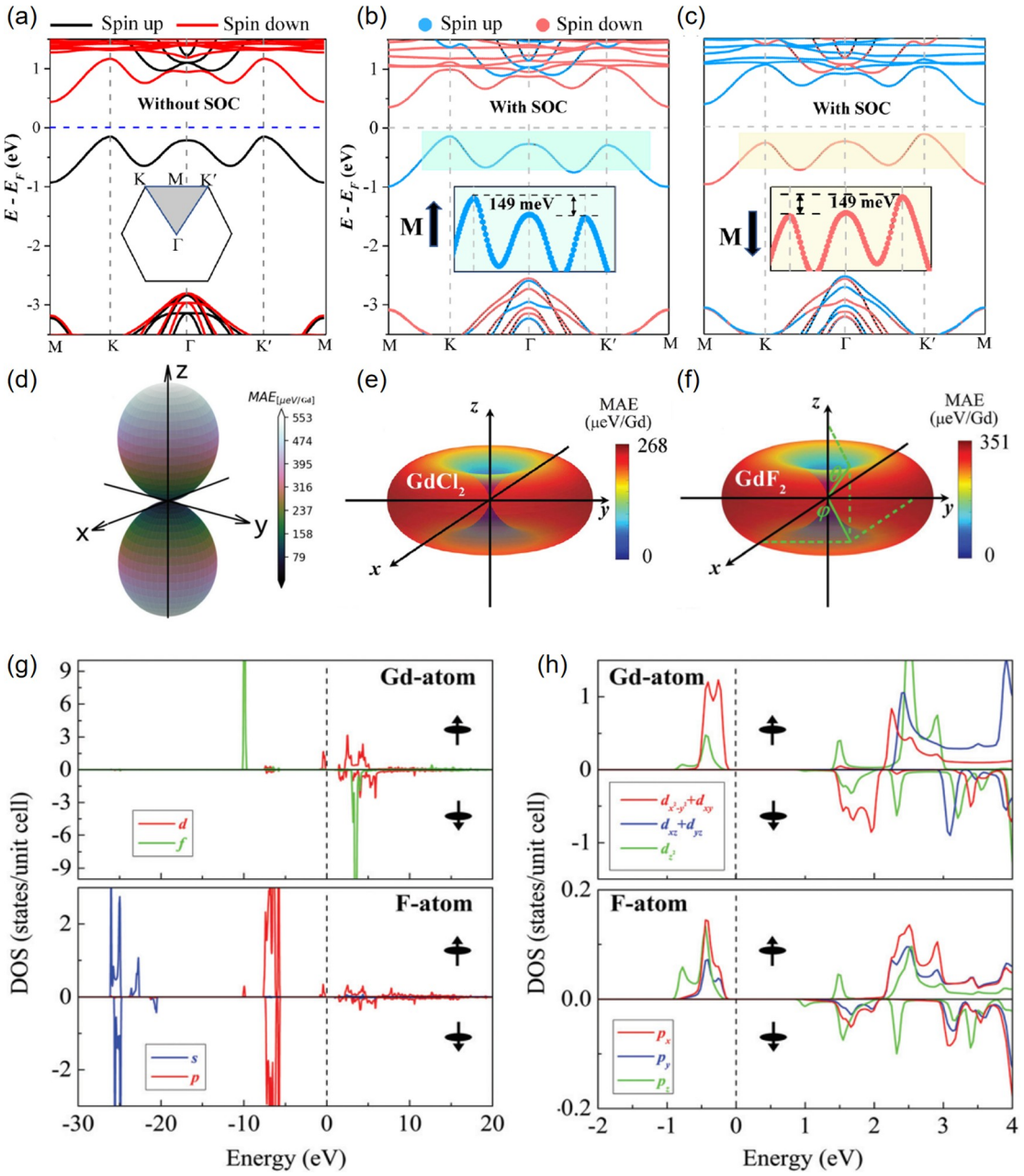


**Figure 2.** Electronic band structure of $GdI_2$ monolayer (a) without SOC and (b, c) with SOC for Gd's magnetic moment along the out-of-plane positive and negative $z$ directions, respectively. (d) Angular dependence of MAE for the $GdI_2$ monolayer with the in-plane MAE set to zero. (e, f) Angular dependence of MAE for the monolayer $GdCl_2$ and $GdF_2$, respectively, with the $z$-direction MAE set to zero. (g, h) Orbital-resolved density of states for monolayer $GdF_2$ with a FM ground state. The Fermi level is set to zero. Parts (a−c) are reproduced with permission from ref 50. Copyright 2021 American Physical Society. Part (d) is reproduced with permission from ref 46. Copyright 2020 Royal Society of Chemistry. Parts (e−h) are reproduced with permission from ref 48. Copyright 2022 Royal Society of Chemistry.

100% spin-polarized carriers by modulating the position of the Fermi level.[46,50] A calculation of the magnetocrystalline anisotropy energy (MAE) demonstrated that the magnetic anisotropy of $GdX_2$ changes from an out-of-plane preference to an in-plane type for X varying from F to I. The $GdI_2$ monolayer exhibits an easy magnetic plane, while $GdF_2$ and $GdCl_2$ monolayers have an out-of-plane easy axis, as illustrated in Figure 2d−f. By using a Monte Carlo (MC) simulation under the energy mapping scheme, all $GdX_2$ monolayers were predicted to possess a large $T_C$ value close to ambient temperature, namely 241 or 251 K for $GdI_2$,[46,47] 229 or 225 K for $GdBr_2$,[47,48] 224 or 245 K for $GdCl_2$,[47,48] and 300 K for $GdF_2$,[48] which are promising for spintronic devices.

The intrinsic ferromagnetism with sizable MAE and high $T_C$ is unexpected for the $GdX_2$ monolayers. With the $GdF_2$ monolayer as an example as illustrated in Figure 2g, Gd's 4f electrons occupy the deep energy levels far away from the Fermi level. These 4f electrons are highly localized due to their narrow and high density distributions. The unexpected ferromagnetism originates from the combined effect of the intra-atomic $Gd_{4f}$−$Gd_{5d}$ coupling and the interatomic $Gd_{5d}$−$Gd_{5d}$ coupling.[46−50] In detail, the Gd ion with a $4f^7 5d^1$ valence electronic configuration contributes a large intrinsic magnetic moment due to the strong


https://doi.org/10.1021/acsaelm.2c00384
ACS Appl. Electron. Mater. 2022, 4, 3168−3176

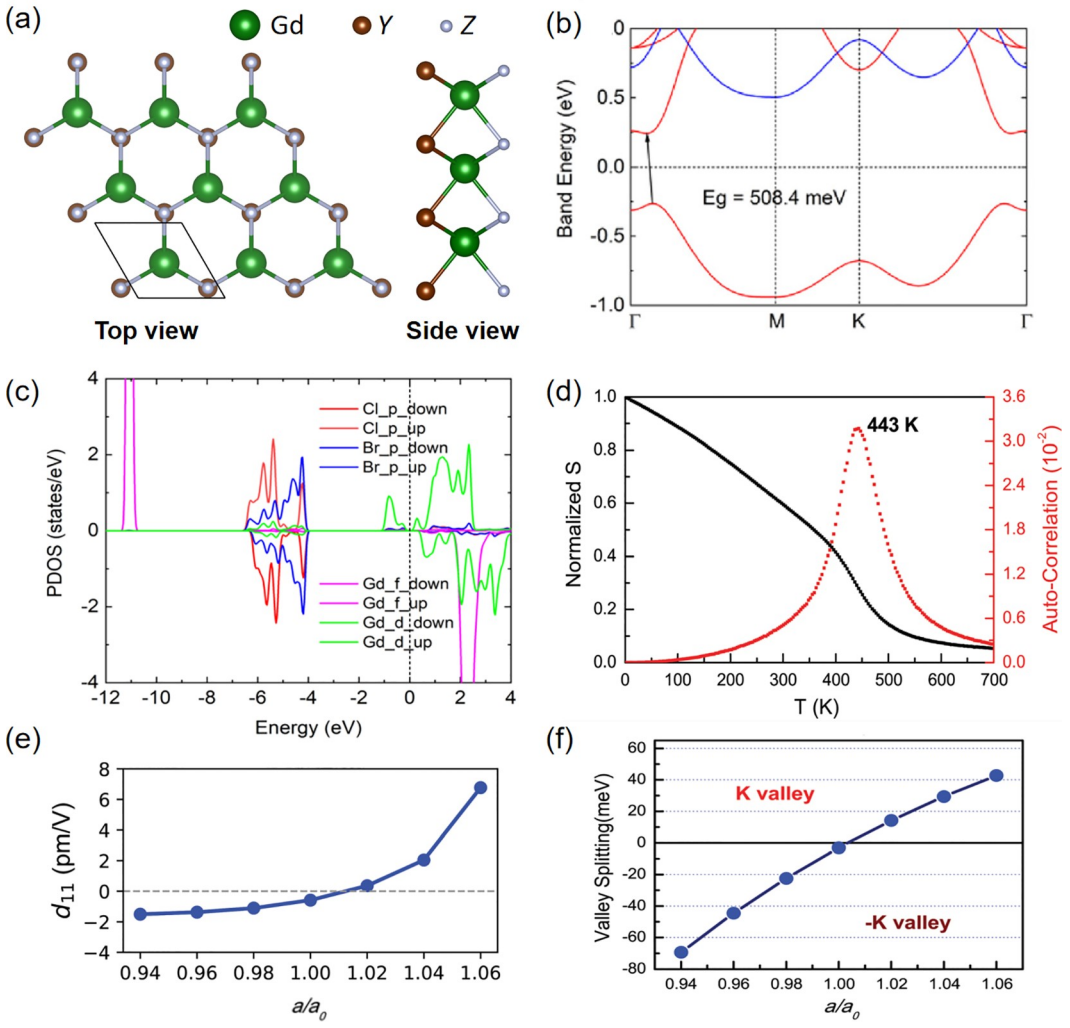


**Figure 3.** (a) Top and side views of the structure for the Janus monolayer GdYZ. (b) Electronic band structure and (c) spin-polarized atom-orbital-projected density of states for the Janus monolayer GdBrCl without the SOC effect. (d) Normalized magnetic moment ($S$) and autocorrelation of the Janus monolayer GdClF as a function of temperature $T$. (e) Piezoelectric strain coefficient $d_{11}$ and (f) the valley splitting as a function of the biaxial strain $a/a_0$ for the Janus monoalyer GdClF, where $a$ and $a_0$ are the strained and unstrained lattice constants, respectively. Parts (b) and (c) are reproduced with permission from ref 51. Copyright 2021 American Institute of Physics. (d–f) are reproduced with permission from ref 52. Copyright 2022 Royal Society of Chemistry.

Hund interaction between 4f and 5d electrons. The top of the valence band is primarily attributed to Gd's 5d orbitals, which appreciably hybridize with p orbitals of X ions, as plotted in Figure 2h. Therefore, the spatially expanded 5d electron acts as a bridge to connect localized 4f electrons, and the robust ferromagnetism is due to effective $Gd_{4f}$–$Gd_{4f}$ interaction mediated by the $Gd_{5d}$–$X_p$–$Gd_{5d}$ exchanges (Figure 1b). The Gd–X–Gd bond angle of close to 90° prefers FM superexchange coupling according to the Goodenough–Kanamori–Anderson (GKA) rule.[59−61] From another perspective, on the basis of a Kramers mechanism, the partially occupied states also lead to a FM direct-exchange interaction between the nearest-neighboring Gd spins.[60]

In addition to charge and spin, the energy valley degrees of freedom have recently attracted considerable attention,[2,62−64] which can also be used as the basis of information coding. The calculations indicated that all $GdX_2$ (X = I, Br, Cl, F) monolayers are ferrovalley materials that have promise for valleytronic applications.[48−50,64] The spontaneous valley splitting reaches 55 or 47.6 meV for $GdF_2$, 38, 35, or 42.3 meV for $GdCl_2$, and 82 or 79 meV for $GdBr_2$, respectively.[48,49,64] In particular, a giant valley splitting of 149 meV was predicted in $GdI_2$ due to its intrinsic ferromagnetism and large SOC.[50] Furthermore, this valley splitting of $GdI_2$ may be even enhanced to about 189 meV at 10% tensile strain.[50] As exhibited in Figure 2b,c, the valley polarization can be flipped by reversing the spin orientation through a moderate external magnetic field. By application of a suitable external electric field, an anomalous valley Hall effect could be realized.[48] It is worth noting that the energy valley in these $GdX_2$ monolayers is mainly contributed by the d electrons of Gd, and a small part from the p electrons of X.[49] Hence, the electrons on Gd's 5d orbitals and the $Gd_{5d}$–$X_p$–$Gd_{5d}$ FM superexchange play important roles in the valley polarization.

## 3. JANUS MONOLAYER BASED ON GADOLINIUM DIHALIDE

Ever since MoSSe was synthesized successfully,[65,66] 2D Janus-type structures have been widely studied. Recently, a few Janus monolayers based on Gd dihalides were predicted by first-principles calculations, i.e. GdClF, GdBrCl, GdICl, and GdIBr



https://doi.org/10.1021/acsaelm.2c00384
ACS Appl. Electron. Mater. 2022, 4, 3168−3176

monolayers,[51,52] which are represented by GdYZ in this paper for convenience of description.

The Janus monolayer GdYZ consists of a Y−Gd−Z sandwich layer akin to the aforementioned $GdX_2$ monolayers, as plotted in Figure 3a. Because of the different atomic sizes and electronegativities of Y and Z, the GdYZ monolayer displays inequivalent Gd−Y and Gd−Z bond lengths, which break the vertical mirror symmetry and bring about a built-in electric field. The AIMD stimulations and phonon spectra confirmed the thermodynamic stability of the GdYZ monolayers.[51,52] The cleavage energies of GdBrCl, GdICl, and GdIBr are 0.203, 0.209, and 0.201 $J/m^2$, respectively,[51] which are smaller than that of graphite, demonstrating the feasibility of exfoliating these GdYZ monolayers from their layered bulks.

All four of these GdYZ monolayers are FM semiconductors with indirect band gaps. The FM order is stable against biaxial strain in the range of −5% to +5%.[51,52] Except for the GdClF monolayer still retains a bipolar magnetic semiconductor characteristic, the other three GdYZ monolayers show the band gap only being determined by the spin-up channel, as illustrated in Figure 3b with GdBrCl as an example. They inherit the intrinsic ferromagnetism of the same origin as for $GdX_2$: namely, the magnetic moment with 8 $\mu_B$/fu mainly comes from half-filled 4f orbitals and partially occupied 5d orbitals ($4f^7$ + $5d^1$). The top of the valence band is primarily attributed to Gd's 5d orbitals, which appreciably hybridize with the p orbitals of Y and Z, playing a key role in their intrinsic ferromagnetism, as plotted in Figure 3c with GdBrCl as an example. Except for GdClF with a perpendicular magnetic anisotropy, GdIBr, GdICl, and GdBrCl monolayers prefer an in-plane magnetic anisotropy. Meanwhile, the strength of the magnetic anisotropy is enhanced by the Janus structure. The MAE values of the GdIBr and GdICl monolayers were predicted to be 708.25 and 613.25 $\mu$eV/Gd, respectively,[51] which are larger than that of $GdI_2$ (553 $\mu$eV/Gd).[46] On the basis of MC simulations, $T_C$ was predicted for these Janus monolayers, namely GdIBr at 167 K, GdICl at 172 K, GdBrCl at 181 K,[51] and a quite high 443 K for GdClF as plotted in Figure 3d,[52] which is desirable for spintronic devices.

In addition, the GdClF monolayer is also a potential ferrovalley material.[52] Although its valley splitting is only −3.1 meV, the valley polarization can be effectively modulated by biaxial strain. The compressive strain can enhance −K valley polarization, while the tensile strain may give rise to K valley polarization. Under a moderate 0.96 compressive strain and 1.04 tensile strain, the corresponding valley splitting energies reach −44.5 and 29.4 meV,[52] respectively (Figure 3f), which can induce an anomalous valley Hall effect tunable by strain. Simultaneously, the strain change from a compressive to a tensile strain can reverse the direction of in-plane piezoelectric polarization (Figure 3e), supplying the probability for a combination of valley properties and piezoelectricity.[52]

## 4. GADOLINIUM TRIHALIDE

In 1960s, bulk $GdI_3$ was experimentally synthesized,[67] which has a vdW layered structure with a hexagonal phase ($R\bar{3}$), as displayed in Figure 4a. The I−Gd−I sandwich layers with 1*T*-$BiI_3$-type structure are stacked along the *c* axis in an ABC sequence. Each Gd ion is caged within an octahedron formed by eight I ions, while the neighboring octahedrons connect in an edge-sharing manner. In comparison with the cleavage energy of graphite, $GdI_3$ has a much lower value (0.12 $J/m^2$),[53] which

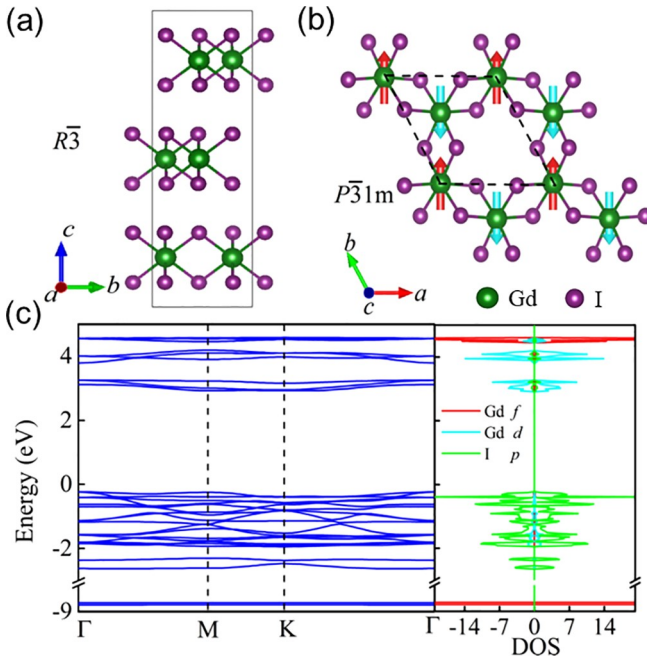


**Figure 4.** (a) Crystal structure of bulk $GdI_3$. (b) Top view of the $GdI_3$ monolayer with a Néel-type-AFM ground state. (c) Band structure and density of states of the $GdI_3$ monolayer. Reproduced with permission from ref 53. Copyright 2021 American Physical Society.

suggests that a $GdI_3$ monolayer with an identical in-plane structure (Figure 4b) can be easily exfoliated from its bulk.

For the $GdI_3$ monolayer, the Néel-type-AFM state (Figure 4b) was verified to be the ground state,[53] which can be easily understood because the half-filled 4f orbitals prefer an AFM coupling according to the Goodenough−Kanamori rule.[59,60] The calculated Gd magnetic moment is very close to the expected value of 7 $\mu_B$/Gd, which comes from its half-filled 4f orbitals. These 4f orbitals of Gd are so localized that the energy difference between FM and AFM states is very small, inducing a quite low Néel temperature. As displayed in Figure 4c, the Néel-type-AFM $GdI_3$ monolayer is a Mott insulator with fully split narrow 4f bands due to a large Hubbard repulsion. The lowest conducting band is contributed by Gd's 5d orbitals, but the highest valence band is contributed by I's 5p orbitals. In comparison with the $4f^7$ + $5d^1$ hybridization in $GdI_2$,[46] $GdI_3$ only possesses a $4f^7$ electronic configuration. The lack of 5d electrons cannot supply an effective medium for $Gd_{4f}$−$Gd_{4f}$ coupling, which is the reason for such a weak exchange. The MAE value is only −0.03 meV/Gd, indicating a weak magnetic anisotropy with an out-of-plane easy axis.[53]

For spintronics applications, it is necessary to tune the magnetism of a $GdI_3$ monolayer. Unfortunately, the usual modulation methods of 2D materials, such as biaxial strain, do not work well on the magnetic properties of the $GdI_3$ monolayer due to its rather localized 4f orbitals. To connect these highly localized 4f orbitals, one efficient route is to introduce electrons to Gd's empty 5d orbitals. Different from the close-packed-triangular structure in $GdI_2$, the honeycomb configuration in $GdI_3$ provides large interstitial positions of hexa-atomic rings to accommodate other atoms. Thereby, electrons doped into Gd's 5d orbitals can be realized by the intercalation of metal atoms.

When Li atoms are inserted into the interstitial positions of $GdI_3$'s hexatomic rings, as shown in Figure 5a, the chemical formula becomes $(GdI_3)_2Li$, which is akin to the intrinsic


https://doi.org/10.1021/acsaelm.2c00384
ACS Appl. Electron. Mater. 2022, 4, 3168−3176

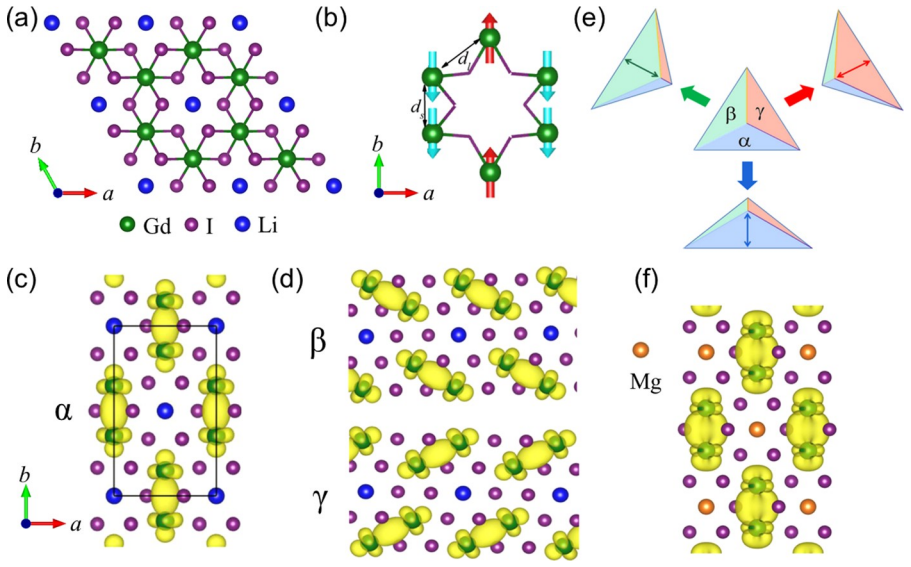


**Figure 5.** (a) Crystal structure of $(GdI_3)_2Li$ monolayer. (b) Gd framework for the stripy-AFM phase. The structural dimerization can be visualized clearly: the shorter bond between parallel-spin pairs and the longer bond between antiparallel-spin pairs. (c) Schematic of Gd's 5d-electron distribution for the $(GdI_3)_2Li$ monolayer, where the electron spindles are along the *b* axis in the $\alpha$ domain. (d) Two other ferroelastic domains ($\beta$ and $\gamma$ domains) with electron spindles along different directions. (e) Deformation of the macroscopic shape of the $(GdI_3)_2Li$ monolayer by external forces. (f) Distribution of electrons for the $(GdI_3)_2Mg$ monolayer. Reproduced with permission from ref 53. Copyright 2021 American Physical Society.

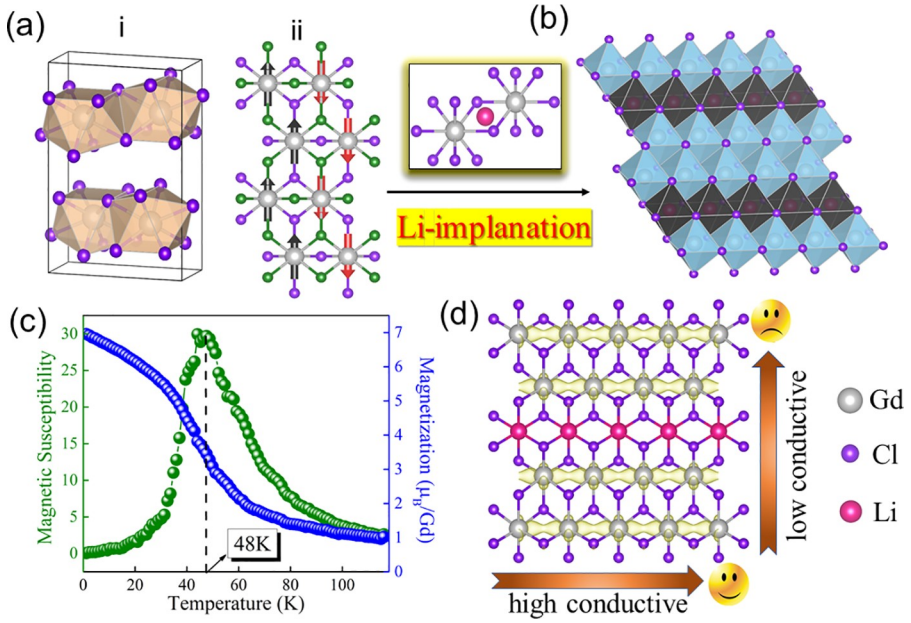


**Figure 6.** (a) (i) Crystal structure of bulk $GdCl_3$ (the *Cmcm* phase) and (ii) a $GdCl_3$ monolayer with a zigzag-type AFM ground state. (b) Structure of $(GdCl_3)_2Li$ after reconstruction induced by the Li implantation. (c) Monte Carlo simulated magnetic susceptibility and magnetization. (d) Electronic density distribution of $(GdCl_3)_2Li$. Reproduced with permission from ref 54. Copyright 2022 Elsevier Ltd.

multiferroic $(CrBr_3)_2Li$ monolayer.[24] Meanwhile, the valence of Gd becomes +2.5 and its magnetic moment is ~7.5 $\mu_B$/Gd. The MAE value of $(GdI_3)_2Li$ is estimated to be 0.46 meV/Gd, preferring an in-plane orientation.[53] The enhanced magnetic anisotropy is due to the strong SOC of Gd's partially filled 5d orbitals.

It is interesting that the one electron introduced from a Li atom generates a Periels transition, namely a strong disproportion of the nearest-neighbor Gd−Gd distances induced by dimerization (Figure 5b), which reduces the symmetry from a honeycomb ($P\bar{3}1m$) to a monoclinic phase ($C2/m$) and triggers a magnetic transition from a Néel-type to a stripy-type AFM state. Due to the strong electron−phonon coupling, a significant ferroelasticity is driven by the Periels transition, making $(GdI_3)_2Li$ a multiferroic monolayer. The Gd's 5d electrons prefer to stay in the middle of the shorter Gd−Gd pair, forming a bond-centered charge ordering such as spindles, as displayed in Figure 5c. This electron spindle leads to a shrunk lattice constant, and thus generates ~4% ferroelastic deformation.[53] Due to the threefold rotational symmetry, the other two similar ferroelastic domains with different orientations of electron spindles are allowed (Figure 5d). The detailed balance among these triple ferroelastic domains can be tuned by external forces along certain directions to reduce mechanical damage,


https://doi.org/10.1021/acsaelm.2c00384
ACS Appl. Electron. Mater. 2022, 4, 3168−3176

that is, the inner strain can be relaxed by rotating the electron spindles and resizing the corresponding ferroelastic domains, as displayed in Figure 5e. This superelasticity offers a great potential for flexible applications.

After Li intercalation, each Gd gains half of an electron from the Li atom. After Mg intercalation, each Gd gains one electron from the Mg atom. In the $(GdI_3)_2Mg$ monolayer, as expected, the valence of Gd becomes +2 and the magnetic moment is ~8 $\mu_B$/Gd.[53] However, the ground state still retains a stripy-AFM phase. Due to more electrons on Gd's 5d orbitals, the value of MAE is enhanced to 1.05 meV with an in-plane preference. Although one electron is doped to each Gd, the multiple 5d orbitals of Gd separate one electron into a half-occupation of two orbitals, as illustrated in Figure 5f, which also leads to the Periels transition and superior ferroelasticity (~9%).[53]

In addition to $GdI_3$, the vdW bulk $GdCl_3$ was synthesized experimentally in the 1960s.[68] Since Cl ions have a stronger electronegativity and smaller ionic radius in comparison to I ions, the Gd−Cl bond is shorter than the Cd−I bond. Hence, the ion cage wrapping each Gd is more compact in $GdCl_3$, forming a rare Cl hendecahedron, which is different from the common octahedron or triangular prism, as shown in Figure 6a. According to our calculations,[54] the $GdCl_3$ monolayer can be easily exfoliated from its bulk. The $GdCl_3$ monolayer possesses a unique orthorhombic structure with hendecahedral ion cages, which is completely different from both the honeycomb structure of $GdI_3$ and the triangular structure of $GdI_2$, representing a brand-new lattice for a 2D magnet.

The $GdCl_3$ monolayer is unique due to not only its structure but also its magnetism. According to the DFT calculation, it is a Mott insulator with a zigzag-type AFM ground state (Figure 6a).[54] By insertion of Li into a Gd−$Cl_2$−Gd interstitial position, a significant structural reconstruction occurs, and exotic Cl hendecahedral cages transform to Cl octahedra (Figure 6b).[54] The symmetry of the resultant $(GdCl_3)_2Li$ monolayer is reduced to monoclinic ($C2/m$). Simultaneously, ferromagnetism is achieved with a large magnetization (7.5 $\mu_B$/Gd) and a moderate $T_C$ value (~48 K) (Figure 6c).[54] Here, the ferromagnetism is induced by doping electrons in Gd's 5d orbitals, via a double-exchange-like process. Namely, the localized 4f moments act as the spin background while the itinerant 5d electrons act as the medium. Moreover, due to the structural anisotropy, the 5d electrons prefer to stay between short Gd−Gd pairs along the $a$ axis, leading to a large electrical transport anisotropy (Figure 6d), which may be peculiarly useful for nanoelectronics.[54]

## 5. CONCLUSION AND OUTLOOK

In this article, we have reviewed a few representative 2D monolayers based on Gd halides with intrinsic 4f magnetism, including the trigonal FM $GdX_2$ family, Janus monolayer GdYZ, honeycomb Néel-type-AFM $GdI_3$, and orthorhombic zigzag-type-AFM $GdCl_3$. For $GdX_2$ and the related Janus monolayer GdYZ, they are all FM semiconductors with high $T_C$ values, which make them promising candidates for spintronic devices. The strong ferromagnetism comes from Gd's localized 4f spins coupled via the spatially expanded 5d electrons. Meanwhile, $GdX_2$ and GdClF are ferrovalley materials, and their spontaneous valley polarizations are mainly contributed by Gd's 5d electrons. For a $GdI_3$ monolayer without an electron on Gd's 5d orbitals, doping a half or single electron into Gd's 5d orbitals can be achieved by Li or Mg intercalation, which leads to a Peierls transition and prominent ferroelasticity. For a $GdCl_3$ monolayer with an exotic structure, Li implanation also dopes electrons into Gd's 5d orbitals, resulting in a significant structural reconstruction, 4f ferromagnetism, and distinctive conductance anisotropy.

In comparison with magnetic materials based on 3d electrons, the magnets based on 4f electrons may provide unique superiorities, such as large local magnetic moment, excellent magnetic anisotropy, and reliable valley polarization, which will supply more possibilities for their use in multifunctional spintronic and valleytronic devices. For this very young topic of 2D 4f magnets, there is still a long way to go before practical applications can be carried out. Although all the studies mentioned above are only theoretical predictions, they imply an effective strategy to take advantage of the highly localized f electrons to improve the magnetism: that is, utilizing the electrons on d orbitals as a medium. This strategy is not limited to Gd halides but is also effective for other Gd-based 2D materials.[69]

Experimentally, monolayers of Gd halides can be obtained using two methods. One method is to synthesize their vdW bulks according to well-established chemical synthesis methods and then to exfoliate monolayers by a mechanical method. The other method is to grow monolayers of Gd halides directly by means of molecular beam epitaxy or vapor transport under gas protection.

In addition to Gd halides, there are also some other 4f magnets existing experimentally which may also have vdW bulks, such as $PrI_3$, $NdI_3$, $TbI_3$, and so on.[67] However, on the theoretical side, it is usually hard for DFT codes such as VASP to deal with their non-half-filled 4f electrons. Thus, up to now the theoretical exploration on these 2D 4f magnets has been very limited.[70] Recently, the electronic structure and magnetic property of $EuX_2$ (X = I, Br, Cl, F) was obtained, since it also has half-filled $4f^7$ orbitals. In addition to its technical convenience, a Gd-based system is the best choice to pursue high-temperature magnetism, on consideration of its cooperative 5d orbitals, which can boost the exchanges between neighboring 4f spins. This is the reason the Gd-based halides have been the first attractive species among all 2D 4f magnets. Even so, more 2D 4f magnets with other rare-earth elements are expected to be studied in the future, with the development of both experimental and theoretical techniques.

## AUTHOR INFORMATION


### Corresponding Authors

**Xiaoyan Yao** − *School of Physics, Southeast University, Nanjing 211189, People's Republic of China*; Email: yaoxiaoyan@seu.edu.cn

**Shuai Dong** − *School of Physics, Southeast University, Nanjing 211189, People's Republic of China*; orcid.org/0000-0002-6910-6319; Email: sdong@seu.edu.cn

### Authors

**Haipeng You** − *School of Physics, Southeast University, Nanjing 211189, People's Republic of China*

**Ning Ding** − *School of Physics, Southeast University, Nanjing 211189, People's Republic of China*

**Jun Chen** − *School of Physics, Southeast University, Nanjing 211189, People's Republic of China*

Complete contact information is available at: https://pubs.acs.org/10.1021/acsaelm.2c00384




https://doi.org/10.1021/acsaelm.2c00384
ACS Appl. Electron. Mater. 2022, 4, 3168−3176

## Notes

The authors declare no competing financial interest.

## ■ ACKNOWLEDGMENTS

This work was supported by the National Natural Science Foundation of China (Grant No. 11834002). We thank the Tianhe-II of National Supercomputer Center in Guangzhou (NSCC-GZ) and the Big Data Center of Southeast University for providing facility support of the numerical calculations.

## ■ REFERENCES

(1) Novoselov, K. S.; Geim, A. K.; Morozov, S. V.; Jiang, D.; Zhang, Y.; Dubonos, S. V.; Grigorieva, I. V.; Firsov, A. A. Electric field effect in atomically thin carbon films. *Science* **2004**, *306*, 666−669.

(2) Xiao, D.; Liu, G.-B.; Feng, W.; Xu, X.; Yao, W. Coupled spin and valley physics in monolayers of $MoS_2$ and other group-VI dichalcogenides. *Phys. Rev. Lett.* **2012**, *108*, 196802.

(3) Manzeli, S.; Ovchinnikov, D.; Pasquier, D.; Yazyev, O. V.; Kis, A. 2D transition metal dichalcogenides. *Nat. Rev. Mater.* **2017**, *2*, 17033.

(4) You, H.-P.; Ding, N.; Chen, J.; Dong, S. Prediction of two-dimensional ferromagnetic ferroelectric $VOF_2$ monolayer. *Phys. Chem. Chem. Phys.* **2020**, *22*, 24109−24115.

(5) Huang, B.; Clark, G.; Klein, D. R.; MacNeill, D.; Navarro-Moratalla, E.; Seyler, K. L.; Wilson, N.; McGuire, M. A.; Cobden, D. H.; Xiao, D.; Yao, W.; Jarillo-Herrero, P.; Xu, X. D. Electrical control of 2D magnetism in bilayer $CrI_3$. *Nat. Nanotechnol.* **2018**, *13*, 544−548.

(6) Ding, N.; Chen, J.; Dong, S.; Stroppa, A. Ferroelectricity and ferromagnetism in a $VOI_2$ monolayer: Role of the Dzyaloshinskii-Moriya interaction. *Phys. Rev. B* **2020**, *102*, 165129.

(7) Lin, L.-F.; Zhang, Y.; Moreo, A.; Dagotto, E.; Dong, S. Frustrated dipole order induces noncollinear proper ferrielectricity in two dimensions. *Phys. Rev. Lett.* **2019**, *123*, 067601.

(8) An, M.; Zhang, Y.; Chen, J.; Zhang, H.-M.; Guo, Y. J.; Dong, S. Tuning magnetism in layered magnet $VI_3$: A theoretical study. *J. Phys. Chem. C* **2019**, *123*, 30545−30550.

(9) Haastrup, S.; Strange, M.; Pandey, M.; Deilmann, T.; Schmidt, P. S.; Hinsche, N. F.; Gjerding, M. N.; Torelli, D.; Larsen, P. M.; Riis-Jensen, A. C.; Gath, J.; Jacobsen, K. W.; Mortensen, J. J.; Olsen, T.; Thygesen, K. S. The Computational 2D Materials Database: high-throughput modeling and discovery of atomically thin crystals. *2D Mater.* **2018**, *5*, 042002.

(10) Gong, C.; Zhang, X. Two-dimensional magnetic crystals and emergent heterostructure devices. *Science* **2019**, *363*, 706−718.

(11) Zhang, J. J.; Lin, L. F.; Zhang, Y.; Wu, M. H.; Yakobson, B. I.; Dong, S. Type-II Multiferroic $Hf_2VC_2F_2$ MXene Monolayer with High Transition Temperature. *J. Am. Chem. Soc.* **2018**, *140*, 9768−9773.

(12) Wang, Z. W.; Ding, N.; Gui, C. R.; Wang, S.-S.; An, M.; Dong, S. Ferroelectricity in strained $Hf_2CF_2$ monolayer. *Phys. Rev. Mater.* **2021**, *5*, 074408.

(13) Kalantar-Zadeh, K.; Ou, J. Z.; Daeneke, T.; Mitchell, A.; Sasaki, T.; Fuhrer, M. S. Two dimensional and layered transition metal oxides. *Appl. Mater. Today* **2016**, *5*, 73−89.

(14) Li, L. K.; Yu, Y. J.; Ye, G. J.; Ge, Q. Q.; Qu, X. D.; Wu, H.; Feng, D. L.; Chen, X. H.; Zhang, Y. B. Black phosphorus field-effect transistors. *Nat. Nanotechnol.* **2014**, *9*, 372−377.

(15) Liu, H.; Neal, A. T.; Zhu, Z.; Luo, Z.; Xu, X.; Tomanek, D.; Ye, P. D. Phosphorene: an unexplored 2D semiconductor with a high hole mobility. *ACS Nano* **2014**, *8*, 4033−4041.

(16) Song, L.; Ci, L. J.; Lu, H.; Sorokin, P. B.; Jin, C. H.; Ni, J.; Kvashnin, A. G.; Kvashin, D. G.; Lou, J.; Yakobson, B. I.; Ajayan, P. M. Large scale growth and characterization of atomic hexagonal boron nitride layers. *Nano Lett.* **2010**, *10*, 3209−3215.

(17) Tan, C. L.; Cao, X. H.; Wu, X.-J.; He, Q. Y.; Yang, J.; Zhang, X.; Chen, J. Z.; Zhao, W.; Han, S. K.; Nam, G. H.; Sindoro, M.; Zhang, H. Recent advances in ultrathin two-dimensional nanomaterials. *Chem. Rev.* **2017**, *117*, 6225−6331.

(18) Huang, C. M.; Wu, S. F.; Sanchez, A. M.; Peters, J. J. P.; Beanland, R.; Ross, J. S.; Rivera, P.; Yao, W.; Cobden, D. H.; Xu, X. D. Lateral heterojunctions within monolayer $MoSe_2$-$WSe_2$ semiconductors. *Nat. Mater.* **2014**, *13*, 1096−1101.

(19) Sun, Y. J.; Zhuo, Z. W.; Wu, X. J.; Yang, J. L. Room-temperature ferromagnetism in two-dimensional $Fe_2Si$ nanosheet with enhanced spin-polarization ratio. *Nano Lett.* **2017**, *17*, 2771−2777.

(20) Zhao, Y. H.; Lin, L. F.; Zhou, Q. H.; Li, Y. H.; Yuan, S. J.; Chen, Q.; Dong, S.; Wang, J. L. Surface vacancy-induced switchable electric polarization and enhanced ferromagnetism in monolayer metal trihalides. *Nano Lett.* **2018**, *18*, 2943−2949.

(21) Sun, Q. L.; Kioussis, N. Prediction of manganese trihalides as two-dimensional Dirac half-metals. *Phys. Rev. B* **2018**, *97*, 094408.

(22) Tang, X.; Kou, L. Z. Two-dimensional ferroics and multiferroics: platforms for new physics and applications. *J. Phys. Chem. Lett.* **2019**, *10*, 6634−6649.

(23) Sun, W.; Wang, W. X.; Li, H.; Zhang, G. B.; Chen, D.; Wang, J. L.; Cheng, Z. X. Controlling bimerons as skyrmion analogues by ferroelectric polarization in 2D van der Waals multiferroic heterostructures. *Nat. Commun.* **2020**, *11*, 5390.

(24) Huang, C. X.; Du, Y. P.; Wu, H. P.; Xiang, H. J.; Deng, K. M.; Kan, E. J. Prediction of intrinsic ferromagnetic ferroelectricity in a transition-metal halide monolayer. *Phys. Rev. Lett.* **2018**, *120*, 147601.

(25) Lee, J. U.; Lee, S.; Ryoo, J. H.; Kang, S.; Kim, T. Y.; Kim, P.; Park, C. H.; Park, J. G.; Cheong, H. Ising-type magnetic ordering in atomically thin $FePS_3$. *Nano Lett.* **2016**, *16*, 7433−7438.

(26) Bhimanapati, G. R.; Lin, Z.; Meunier, V.; Jung, Y.; Cha, J.; Das, S.; Xiao, D.; Son, Y.; Strano, M. S.; Cooper, V. R.; Liang, L. B.; Louie, S. G.; Ringe, E.; Zhou, W.; Kim, S. S.; Naik, R. R.; Sumpter, B. G.; Terrones, H.; Xia, F. N.; Wang, Y. L.; Zhu, J.; Akinwande, D.; Alem, N.; Schuller, J. A.; Schaak, R. E.; Terrones, M.; Rhbinson, J. A. Recent advances in two-dimensional materials beyond graphene. *ACS Nano* **2015**, *9*, 11509−11539.

(27) O'Hara, D. J.; Zhu, T. C.; Trout, A. H.; Ahmed, A. S.; Luo, Y. K.; Lee, C. H.; Brenner, M. R.; Rajan, S.; Gupta, J. A.; McComb, D. W.; Kawakami, R. K. Room temperature intrinsic ferromagnetism in epitaxial manganese selenide films in the monolayer limit. *Nano Lett.* **2018**, *18*, 3125−3131.

(28) Jiang, X.; Liu, Q.; Xing, J.; Liu, N.; Guo, Y.; Liu, Z.; Zhao, J. Recent progress on 2D magnets: Fundamental mechanism, structural design and modification. *Appl. Phys. Rev.* **2021**, *8*, 031305.

(29) Guo, Y.; Zhou, S.; Zhao, J. J. Two-dimensional intrinsic ferromagnets with high Curie temperatures: synthesis, physical properties and device applications. *J. Mater. Chem. C* **2021**, *9*, 6103.

(30) Yao, X.; Wang, Y.; Dong, S. Noncollinear topological textures in two-dimensional van der Waals materials: From magnetic to polar systems. *Int. J. Mod. Phys. B* **2021**, *35*, 2130004.

(31) Liu, L.; Pai, C.-F.; Li, Y. H.; Tseng, H. W.; Ralph, D. C.; Buhrman, R. A. Spin-torque switching with the giant spin Hall effect of tantalum. *Science* **2012**, *336*, 555−558.

(32) Han, W.; Kawakami, R. K.; Gmitra, M.; Fabian, J. Graphene spintronics. *Nat. Nanotechnol.* **2014**, *9*, 794−807.

(33) Gupta, A.; Sakthivel, T.; Seal, S. Recent development in 2D materials beyond graphene. *Prog. Mater. Sci.* **2015**, *73*, 44−126.

(34) Huang, C. X.; Feng, J. S.; Wu, F.; Ahmed, D.; Huang, B.; Xiang, H. J.; Deng, K. M.; Kan, E. J. Toward intrinsic room-temperature ferromagnetism in two-dimensional semiconductors. *J. Am. Chem. Soc.* **2018**, *140*, 11519−11525.

(35) Jansen, R. Silicon spintronics. *Nat. Mater.* **2012**, *11*, 400−408.

(36) Huang, B.; Clark, G.; Navarro-Moratalla, E.; Klein, D. R.; Cheng, R.; Seyler, K. L.; Zhong, D.; Schmidgall, E.; McGuire, M. A.; Cobden, D. H.; Yao, W.; Xiao, D.; Jarillo-Herrero, P.; Xiao, X. D. Layer-dependent ferromagnetism in a van der Waals crystal down to the monolayer limit. *Nature* **2017**, *546*, 270−273.

(37) Gong, C.; Li, L.; Li, Z.; Ji, H.; Stern, A.; Xia, Y.; Cao, T.; Bao, W.; Wang, C.; Wang, Y.; Qiu, Z. Q.; Cava, R. J.; Louie, S. G.; Xia, J.; Zhang, X. Discovery of intrinsic ferromagnetism in two-dimensional van der Waals crystals. *Nature* **2017**, *546*, 265−269.

(38) Deng, Y. J.; Yu, Y. J.; Song, Y. C.; Zhang, J. Z.; Zhang, J. Z.; Wang, N. Z.; Sun, Z. Y.; Yi, Y. F.; Wu, Y. Z.; Wu, S. W.; Zhu, J. Y.; Wang, J.;



https://doi.org/10.1021/acsaelm.2c00384
ACS Appl. Electron. Mater. 2022, 4, 3168−3176

Chen, X. H.; Zhang, Y. B. Gate-tunable room-temperature ferromagnetism in two-dimensional $Fe_3GeTe_2$. *Nature* **2018**, *563*, 94−99.
(39) Bonilla, M.; Kolekar, S.; Ma, Y. J.; Diaz, H. C.; Kalappattil, V.; Das, R.; Eggers, T.; Gutierrez, H. R.; Phan, M. H.; Batzill, M. Strong room temperature ferromagnetism in $VSe_2$ monolayers on van der Waals substrates. *Nat. Nanotechnol.* **2018**, *13*, 289−293.
(40) Sivadas, N.; Daniels, M. W.; Swendsen, R. H.; Okamoto, S.; Xiao, D. Magnetic ground state of semiconducting transition-metal trichalcogenide monolayers. *Phys. Rev. B* **2015**, *91*, 235425.
(41) Wang, S.; Miao, N.; Su, K.; Blatov, V. A.; Wang, J. Discovery of intrinsic two-dimensional antiferromagnets from transition-metal borides. *Nanoscale* **2021**, *13*, 8254−8263.
(42) Wang, B.; Zhang, Y. H.; Ma, L.; Wu, Q. S.; Guo, Y. L.; Zhang, X. W.; Wang, J. X. MnX (X= P, As) monolayers: a new type of two-dimensional intrinsic room temperature ferromagnetic half-metallic material with large magnetic anisotropy. *Nanoscale* **2019**, *11*, 4204−4209.
(43) An, M.; Dong, S. Ferroic orders in two-dimensional transition/rare-earth metal halides. *APL Mater.* **2020**, *8*, 110704.
(44) Zhao, M. Y.; Chen, J.; Wang, S. S.; An, M.; Dong, S. Multiferroic properties of oxygen-functionalized magnetic i-MXene. *Phys. Rev. Mater.* **2021**, *5*, 094408.
(45) Huang, F. T.; Cheong, S. W. Aperiodic topological order in the domain configuration of functioncal materials. *Nat. Rew. Mater.* **2017**, *2*, 17004.
(46) Wang, B.; Zhang, X. W.; Zhang, Y. H.; Yuan, S. J.; Guo, Y. L.; Dong, S.; Wang, J. L. Prediction of two-dimensional high-$T_c$ *f*-electron ferromagnetic semiconductor. *Mater. Horiz.* **2020**, *7*, 1623−1630.
(47) Liu, W. Q.; Tong, J. W.; Deng, L.; Yang, B.; Xie, G. M.; Qin, G. W.; Tian, F. B.; Zhang, X. M. Two-dimensional ferromagnetic semiconductors of rare-earth monolayer $GdX_2$ ($X$ = Cl, Br, I) with large perpendicular magnetic anisotropy and high Curie temperature. *Mater. Today Phys.* **2021**, *21*, 100514.
(48) Sheng, K.; Yuan, H.; Wang, Z.-Y. Monolayers gadolinium halides $GdX_2$ ($X$ = F, Cl, Br): intrinsic ferrovalley materials with spontaneous spin and valley polarizations. *Phys. Chem. Chem. Phys.* **2022**, *24*, 3865−3874.
(49) Ding, F.; Ji, S. L.; Li, S. S.; Wang, L. X.; Wu, H.; Hu, Z. F.; Li, F. Prediction of intrinsic valley polarization in single-layer $GdX_2$ ($X$=Br, Cl) from a first-principles study. *Phys. Status Solidi* **2021**, *258*, 2100356.
(50) Cheng, H.-X.; Zhou, J.; Ji, W.; Zhang, Y.-N.; Feng, Y.-P. Two-dimensional intrinsic ferrovalley $GdI_2$ with large valley polarization. *Phys. Rev. B* **2021**, *103*, 125121.
(51) Li, S. J.; Jiang, W.; Hou, Y. F.; Zheng, F. W.; Shao, X. H.; Zhang, P. High curie temperatures in Gd-dihalide Janus monolayers. *J. Appl. Phys.* **2021**, *130*, 043902.
(52) Guo, S.-D.; Guo, X.-S.; Cai, X.-X.; Liu, B.-G. Valley polarization transition driven by biaxial strain in Janus GdClF monolayer. *Phys. Chem. Chem. Phys.* **2022**, *24*, 715−723.
(53) You, H. P.; Zhang, Y.; Chen, J.; Ding, N.; An, M.; Miao, L.; Dong, S. Peierls transition driven ferroelasticity in the two-dimensional *d-f* hybrid magnets. *Phys. Rev. B* **2021**, *103*, L161408.
(54) You, H. P.; Chen, J.; Zhang, J. J.; Ding, N.; Zhang, X. W.; Yao, X. Y.; Dong, S. Structural reconstruction and anisotropic conductance in 4f-ferromagnetic monolayer. *Mater. Today Phys.* **2022**, *24*, 100693.
(55) Mee, J. E.; Corbett, J. D. Rare Earth Metal-Metal Halide Systems. VII. The Phases Gadolinium 1.6-Chloride and Gadolinium Diiodide. *Inorg. Chem.* **1965**, *4*, 88−93.
(56) Taraphder, A.; Laad, M. S.; Craco, L.; Yaresko, A. N. $GdI_2$: A New Ferromagnetic Excitonic Solid? *Phys. Rev. Lett.* **2008**, *101*, 136410.
(57) Ryazanov, M.; Simon, A.; Kremer, R. K. Magnetic freezing and spin frustration in the triangular lattice magnets $GdI_2H_x$ ($0 \leq x < 1$). *Phys. Rev. B* **2008**, *77*, 104423.
(58) Kasten, A.; Müller, P. H.; Schienle, M. Magnetic ordering in $GdI_2$. *Solid. State. Commun.* **1984**, *51*, 919−921.
(59) Goodenough, J. B. Theory of the role of covalence in the perovskite-type manganites [La, M (II)]$MnO_3$. *Phys. Rev.* **1955**, *100*, 564.
(60) Kanamori, J.; Moriya, T.; Motizuki, T.; Nagamiya, T. Methods of calculating the crystalline electric field. *J. Phys. Soc. Jpn.* **1955**, *10*, 93−102.
(61) Anderson, P. W. New approach to the theory of superexchange interactions. *Phys. Rev.* **1959**, *115*, 2−13.
(62) Cao, T.; Wang, G.; Han, W. P.; Ye, H. Q.; Zhu, C. R.; Shi, J. R.; Niu, Q.; Tan, P. H.; Wang, E.; Liu, B. L.; Feng, J. Valley-selective circular dichroism of monolayer molybdenum disulphide. *Nat. Commun.* **2012**, *3*, 1−5.
(63) Zeng, H.; Dai, J.; Yao, W.; Xiao, D.; Cui, X. Valley polarization in $MoS_2$ monolayers by optical pumping. *Nat. Nanotechnol.* **2012**, *7*, 490−493.
(64) Guo, S. D.; Zhu, J. X.; Mu Wen, Q.; Liu, B. G. Possible way to achieve anomalous valley Hall effect by piezoelectric effect in a $GdCl_2$ monolayer. *Phys. Rev. B* **2021**, *104*, 224428.
(65) Lu, A.-Y.; Zhu, H. Y.; Xiao, J.; Chuu, C.-P.; Han, Y. M.; Chiu, M.-H.; Cheng, C.-C.; Yang, C.-W.; Wei, K.-H.; Yang, Y. M.; Wang, Y.; Sokaras, D.; Nordlund, D.; Yang, P. D.; Muller, D. A.; Chou, M. Y.; Zhang, X.; Li, L. J. Janus monolayers of transition metal dichalcogenides. *Nat. Nanotechnol.* **2017**, *12*, 744−749.
(66) Zhang, J.; Jia, S.; Kholmanov, I.; Dong, L.; Er, D. Q.; Chen, W. B.; Guo, H.; Jin, Z. H.; Shenoy, V. B.; Shi, Li; Lou, J. Janus monolayer transition-metal dichalcogenides. *ACS Nano* **2017**, *11*, 8192−8198.
(67) Asprey, L. B.; Keenan, T. K.; Kruse, F. H. Preparation and crystal data for lanthanide and actinide triiodides. *Inorg. Chem.* **1964**, *3*, 1137−1141.
(68) Harris, A. L.; Veale, C. R. Polymorphism in gadolinium trichloride. *J. Inorg. Nucl. Chem.* **1965**, *27*, 1437−1439.
(69) Wang, Y. W.; Cui, Z. C.; Zeng, H. H.; Wang, Z. J.; Zhang, X.; Shi, J. Q.; Cao, T. F.; Fan, X. L. Tunable magnetic order in two-dimensional layered $GdGe_2$. *J. Mater. Chem. C* **2022**, *10*, 1259.
(70) Sheng, K.; Chen, Q.; Yuan, H. K.; Wang, Z. Y. Monolayer $CeI_2$: An intrinsic room-temperature ferrovalley semiconductor. *Phys. Rev. B* **2022**, *105*, 075304.




https://doi.org/10.1021/acsaelm.2c00384
*ACS Appl. Electron. Mater.* 2022, 4, 3168−3176